

Magnetic, thermal, and magnetocaloric properties of the holmium trialuminide HoAl_3 with polytypic phases

Takafumi D. Yamamoto^{a,*}, Pedro Baptista de Castro^{a,b}, Kensei Terashima^a,
Akiko T. Saito^a, Hiroyuki Takeya^a, Yoshihiko Takano^{a,b}

^aNational Institute for Materials Science, Tsukuba, Ibaraki 305-0047, Japan

^bUniversity of Tsukuba, Tsukuba, Ibaraki 305-8577, Japan

Abstract

We investigate the magnetic, thermal, and magnetocaloric properties of the intermetallic HoAl_3 compounds with two different crystal structures. The room-temperature equilibrium trigonal phase HoAl_3 undergoes an antiferromagnetic (AFM) transition at the Néel temperature $T_N^{\text{tri}} = 9.8$ K. The AFM ordering of the compound is strong against the magnetic field, so that inverse magnetocaloric effect (MCE) is found even under a magnetic field change of 0–50 kOe. The high-pressure cubic phase HoAl_3 , prepared by a rapid-solidification process, is antiferromagnetically ordered below $T_N^{\text{cub}} = 15$ K. Magnetic and specific heat measurements reveal that this long-range AFM state becomes unstable as the temperature drops and then it is replaced by a magnetic glassy state below a spin freezing temperature $T_f = 11$ K. The successive changes in magnetic state result in complicated temperature and field dependence of the MCE at low temperatures.

Keywords: Rare-earth aluminide, Rapid-solidification, Magnetocaloric effect, Magnetic properties

*Corresponding author

Email address: YAMAMOTO.Takafumi@nims.go.jp (Takafumi D. Yamamoto)

1. Introduction

Magnetocaloric effect is a magneto-thermodynamic phenomenon in which a magnetic material absorbs/generates heat when an applied magnetic field changes. It is often characterized by the isothermal magnetic entropy change ΔS_M . Since the discovery of the giant MCE of $\text{Gd}_5\text{Si}_2\text{Ge}_2$ in 1997 [1], much effort has been put into searching for magnetic materials with large MCEs, the so-called magnetocaloric materials, owing to their potential application to magnetic refrigeration near room temperature [2–4]. Recently, with the growing interest in magnetic refrigerators for liquefaction of nitrogen, hydrogen, and helium, magnetocaloric materials for low temperature applications have been enthusiastically investigated for a wide range of materials, from rare-earth based alloys [5–10] to rare-earth based oxides [11–15].

Binary holmium aluminide is one of a series of compounds that has been widely studied in the context of magnetocaloric material exploration. Among them, HoAl_2 is possibly the most well-known compound, exhibiting a large ΔS_M of $-28.8 \text{ J kg}^{-1} \text{ K}^{-1}$ at the Curie temperature $T_C \sim 30 \text{ K}$ for a magnetic field change ΔH of 50 kOe [16]. These characteristics make this compound a promising candidate for magnetic refrigerants for hydrogen liquefaction. HoAl and Ho_3Al_2 are also reported as candidates for low-temperature magnetic refrigerants [17, 18]. The maximum value of ΔS_M are $-22.5 \text{ J kg}^{-1} \text{ K}^{-1}$ at $T_C = 20 \text{ K}$ for HoAl and $-18.7 \text{ J kg}^{-1} \text{ K}^{-1}$ at $T_C = 40 \text{ K}$ for Ho_3Al_2 for $\Delta H = 50 \text{ kOe}$, respectively. Besides, Ho_2Al is known to show multiple magnetic transitions at 40 K and 13 K, with the maximum ΔS_M of $-6.9 \text{ J kg}^{-1} \text{ K}^{-1}$ around 30 K for $\Delta H = 50 \text{ kOe}$ [19]. Curiously, as far as we know, only the trialuminide HoAl_3 has not yet been clarified in terms of the magnetocaloric properties.

The crystal structure of RAl_3 ($R = \text{Rare-earth}$) has been investigated in detail, and it is known that it changes with the temperature, pressure, and atomic number of the rare-earth elements [20, 21]. In contrast, little information is available on their magnetism, only revealing that the room-temperature equilibrium phase RAl_3 are antiferromagnets with the Néel temperature T_N of 20 K or less [22]. Meanwhile, it has been suggested that the high-pressure phase RAl_3 ($R = \text{Dy, Ho, and Er}$) are ferromagnets with MCEs comparable RAl_2 [23]. These RAl_3 systems in this work, however, are reported as impurity phases in Al-rich RAl_2 compounds, so the physical properties of themselves still have room for verification.

In this study, we comprehensively investigate on the magnetic, thermal, and magnetocaloric properties of HoAl_3 for both the room-temperature equilibrium phase and the high-pressure phase. As shown in Fig. 1, the former has the HoAl_3 -type trigonal structure with the space group of $R\bar{3}m$, and the latter has the Cu_3Au -type cubic structure with the space group of $Pm\bar{3}m$. Here we attempt to synthesize the cubic phase HoAl_3 by a rapid-solidification process in the trigonal phase

HoAl₃, referring that high-pressure conditions have been simulated in the rapidly solidified DyAl₃ [25]. The obtained samples are examined in terms of the crystal structure, phase fraction, and physical properties.

2. Material and Methods

Starting material was prepared by arc-melting from Ho metal (3N) and Al metal (4N). To avoid the appearance of HoAl₂ [26], non-stoichiometric amounts of these reagents—Ho: Al = 15 at. %: 85 at. %—were melted and flipped several times in an arc-melting furnace under an argon atmosphere. The rapid-solidification process was performed for the arc-melted alloy by using another arc-melting furnace equipped with a copper hammer set. A piece of the alloy 3–5 mm in size was placed on the copper hearth, arc-melted again under an argon atmosphere, and then rapidly quenched by hitting it with the hammer. The splattered samples were collected for measurements. Powder X-ray diffraction (XRD) measurements were performed using a Rigaku MiniFlex600 diffractometer with Cu- $K\alpha$ radiation. The XRD data were analyzed by a Rietveld refinement method using the XERUS open-source package [27]. The energy-dispersive X-ray spectroscopy (EDS) analysis was performed to confirm element distribution of the samples by using a JEOL JSM-6010LA scanning electron microscope (SEM) operated at 20 kV. Magnetization (M) measurements were carried out by a Quantum Design SQUID magnetometer. Specific heat (C) data were collected by a thermal relaxation method with a Quantum Design PPMS's option. The same sample was used in these physical property measurements.

3. Results and discussion

3.1. Sample characterization

Figures 2(a) and 2(b) shows the powder XRD patterns of the arc-melted HoAl₃ and the rapidly quenched HoAl₃. The results demonstrate that the diffraction pattern is completely different before and after the rapid-solidification process. The main peaks can be assigned to the trigonal structure for the arc-melted sample and to the cubic structure for the rapidly quenched sample. Thus, it is confirmed that the rapid-solidification process causes the transformation of the crystal structure of HoAl₃, from the room-temperature equilibrium trigonal phase to the high-pressure cubic phase. In this regard, the cubic phase HoAl₃ can be regarded as a metastable phase. Besides, the change in crystal structure of HoAl₃ by the rapid quenching is highly reproducible.

The Rietveld refinement reveals that each sample contains impurity phases: 27 wt. % of Al phase for both samples and 3 wt. % of HoAl₂ phase for the rapidly quenched sample. The presence of a large amount of Al phase is in consequence

of the Al-rich nominal composition ratio. The HoAl_2 phase was not found in the arc-melted sample by the Rietveld refinement, implying that the weight fraction is less than 1%. Hereafter, we refer the arc-melted sample and the rapidly quenched one to trigonal HoAl_3 and cubic HoAl_3 , respectively.

The SEM secondary electron images and the corresponding EDS mapping images for Ho and Al elements are shown in Figs. 3(a)-(f) for each sample. The trigonal HoAl_3 has Al-rich regions and Ho-rich regions. The composition analysis at several positions reveals that the former areas have 93–99 at.% of Al element. On the other hand, the composition ratio in the latter areas is evaluated to be Ho: Al = 27.5 at.%: 72.5 at.%, roughly corresponding to HoAl_3 . Consequently, it is evident that the excess Al phase and the HoAl_3 phase are well-separated each other in the trigonal HoAl_3 . Meanwhile, such phase separation is less visible in the cubic HoAl_3 , especially as can be seen from Fig. 3(f). The composition ratio approximately agrees with the nominal composition, Ho: Al = 15 at.%: 85 at.%, over the entire region. The excess Al phase and the HoAl_3 phase seem to be homogeneously distributed in the cubic HoAl_3 .

Here we will mention the influences of the impurity phases on the thermodynamic properties of the sample. The ferromagnetic HoAl_2 phase may contribute to both the magnetization and the specific heat. The non-magnetic Al phase would not contribute to the former at least in the low-temperature region, but it may have a significant contribution to the latter. The primary influence of the excess Al phase is to largely reduce the phase fraction of HoAl_3 phase. Accordingly, the observed values of the thermodynamic quantities are lower than the real values for the studied compounds. In this paper, the thermodynamic property data are given in weight units using the total mass of the sample. By combining these data with the weight fraction of the impurity phases, one can estimate the real values of the thermodynamic quantities of HoAl_3 phase.

3.2. Magnetic properties of trigonal HoAl_3

Figure 4(a) shows the temperature dependence of the magnetic susceptibility (M/H) of the trigonal HoAl_3 at 0.1 kOe in zero field cooling (ZFC) and field cooling (FC) processes. The sample was cooled down to 2 K in zero magnetic field before measuring the ZFC curve, and then the magnetization data was taken at 0.1 kOe while heating up to 40 K. Subsequently, the FC curve was measured while cooling under the same magnetic field. A sharp cusp is observed at about 10 K, being attributed to the occurrence of an AFM ordering reported in the literature [22]. The Néel temperature T_N^{tri} , defined as the cusp temperature, is evaluated to be 9.8 K. This is consistent with the literature values. As shown in Fig. 4(b), the cusp is well-defined even in higher magnetic fields, and the cusp temperature is slightly decreased down to about 8.3 K at 50 kOe. These results suggest that the AFM ordering of the trigonal HoAl_3 is strong against the magnetic field.

One finds that M/H below the cusp temperature suddenly increases between 20 kOe and 30 kOe and then becomes temperature-independent at 50 kOe. For further investigation on this point, we measured the field dependence of the magnetization. Figure 4(c) shows the results at several temperatures. The magnetization exhibits a linear field dependence at above 10 K, whereas non-monotonical behavior is seen at even lower temperatures. To make this clear, we show the field derivative dM/dH at various temperatures in Fig. 4(d). It is found that a broad peak appears around 25 kOe at below 9 K and becomes pronounced with decreasing temperature. These results imply a field-induced magnetic transition in the trigonal HoAl_3 , but the nature of which is to be further examined. Nevertheless, at least the system seems not to be in a (forced) ferromagnetic state even at 50 kOe because the temperature dependence of M/H at 50 kOe is different from what is expected in such cases [28].

We notice a small difference at below 15 K between ZFC and FC curves at 0.1 kOe. One may consider that it is due to a tiny amount of the ferromagnetic impurity HoAl_2 , but this possibility can be ruled out. According to the literature [29], if this was the case, $M/H-T$ curves should exhibit an anomaly near the Curie temperature of HoAl_2 (~ 30 K). The origin is unclear at the present stage. Nonetheless, we will mention that no difference is found at above 1 kOe (not shown).

3.3. Magnetic properties of cubic HoAl_3

Figure 5(a) shows the temperature dependence of M/H of the cubic HoAl_3 measured at 0.1 kOe in ZFC and FC processes. Unlike the trigonal HoAl_3 , the M/H of the cubic HoAl_3 exhibits two anomalies, namely, a kink at 15 K and a cusp at 11 K. As shown in Fig. 5(b), the kink is clearly observed even in higher magnetic fields, and the kink temperature is only decreased by 0.9 K at 50 kOe. These characteristics resemble to those of the cusp observed in the trigonal HoAl_3 , so it is expected that the kink at 15 K does originate from an AFM transition. On the other hand, the cusp of the cubic HoAl_3 becomes obscured with increasing H and disappears at above 20 kOe. Moreover, a large difference between ZFC and FC curves is observed below the cusp temperature. These results are quite different from those of the trigonal HoAl_3 , suggesting that the cusp of the cubic HoAl_3 at 11 K is not due to an AFM transition, but rather can be ascribed to the occurrence of other magnetic states. Note that no trace of HoAl_2 phase is found in $M/H-T$ curves near 30 K.

One can also find additional signs of a change in magnetic state of cubic HoAl_3 from the field dependence of the magnetization. As shown in Fig. 5(c), the magnetization shows a monotonical field dependence at 2 K, unlike the trigonal HoAl_3 . Furthermore, a broad peak of dM/dH is observed around 30 kOe between 10 K and 13 K, whereas it disappears at below 8 K (see Fig. 5(d)). These results imply

that the magnetic state of the cubic HoAl₃ is no longer in an AFM state as the temperature decreases.

3.4. Thermal properties

Figure 6(a) shows the temperature dependence of C at 0 kOe for the trigonal HoAl₃ and the cubic HoAl₃. The specific heat data for pure Al, which was taken by ourselves, is also represented by scaling with the weight fraction of 0.27. The trigonal HoAl₃ exhibits a sharp specific heat peak near 10 K, being associated with the AFM transition at T_N^{tri} . By applying the magnetic field, the peak is slightly shifted to lower temperatures, as shown in Fig. 6(b). This corresponds to the decrease in cusp temperature of M/H . The C of the cubic HoAl₃ at 0 kOe has a similar peak near 15 K. Moreover, as shown in Fig. 6(c), a slight peak shift with increasing H is also observed. From the similarity between these two specific heat peaks, we conclude that the cubic HoAl₃ undergoes an AFM transition at the Néel temperature $T_N^{\text{cub}} = 15$ K. The large specific heat peaks near T_N guarantees that the HoAl₃ phase is the main phase of each sample used for the physical property measurements. As expected above, 27 wt.% of Al phase has a significant contribution to the specific heat at above 20 K, while it can be negligible at even lower temperatures. The contribution from the HoAl₂ phase is not observed in both the samples.

For the cubic HoAl₃, no specific heat peak is found at 11 K despite the clear cusp of M/H is observed at 0.1 kOe at this temperature. This discrepancy between C and M/H strongly suggests the occurrence of a magnetic glassy state at 11 K in this compound [30]. To get more insight into the ground state, we performed the magnetization relaxation measurement. Here, the sample was first cooled down to 2 K at 0 kOe and magnetized by the magnetic field of 50 kOe. The magnetic field was then switched off after waiting for 5 minutes, and finally a magnetic relaxation curve was measured at 0 kOe. As can be seen from Fig. 6(d), the magnetization continues to decrease over a long period of time. This result also supports the presence of a magnetic glassy state. Therefore, it is revealed that the magnetic state of the cubic HoAl₃ changes from a long-range AFM ordered state to a magnetic glassy state at a spin freezing temperature T_f of 11 K. The nature and the origin of the magnetic glassy state are to be further verified in a single-phase polycrystalline sample or a single crystal.

3.5. Magnetocaloric properties

Now let us evaluate the magnetocaloric properties of the two compounds. In this study, we calculate the magnetic entropy change ΔS_M from the specific heat data by using the expression,

$$\Delta S_M(\Delta H, T) = S(H, T) - S(0, T) = \int_0^T \frac{C(H, T)}{T} dT - \int_0^T \frac{C(0, T)}{T} dT. \quad (1)$$

Figure 7(a) shows the temperature dependence of ΔS_M of the trigonal HoAl_3 for $\Delta H = 10, 30,$ and 50 kOe. At the temperature above $T_N^{\text{tri}} = 9.8$ K, negative ΔS_M increases in magnitude with decreasing temperature and is maximized at just above T_N^{tri} . The maximum value is about $-2.6 \text{ J kg}^{-1} \text{ K}^{-1}$ for $\Delta H = 50$ kOe. This is a conventional MCE expected in the paramagnetic region, which reflects the release of the magnetic entropy as the paramagnetic moments are aligned by a magnetic field. As the temperature further drops, ΔS_M rapidly changes the sign to positive, peaks near T_N^{tri} in each magnetic field, and then goes to zero. The maximum value is about $+2.0 \text{ J kg}^{-1} \text{ K}^{-1}$ for $\Delta H = 50$ kOe. The positive ΔS_M means the restoration of magnetic entropy by applying the magnetic field. This phenomenon—inverse MCE—is generally expected in AFM materials [31, 32], being associated with antiparallel disorder of magnetic sublattices [33].

The ΔS_M - T curves of the cubic HoAl_3 are shown in Figure 7(b). The conventional MCE is observed in the paramagnetic region at above $T_N^{\text{cub}} = 15$ K. The maximum negative value of ΔS_M is about $-3.3 \text{ J kg}^{-1} \text{ K}^{-1}$ for $\Delta H = 50$ kOe. Although ΔS_M drops towards a positive value with further decreasing temperature, the fall stops immediately and the significant positive ΔS_M peak is never found. This is in quite contrary to the expectation that like the trigonal HoAl_3 , an inverse MCE appears at below T_N^{cub} in response to the disruption of a long-range AFM order by the magnetic field. Instead, a hump appears around $T_f = 11$ K and contributes to ΔS_M as a negative component, of which the magnitude increases with increasing ΔH . The replacement of the expected positive ΔS_M peak by the hump also supports that a long-range AFM order no longer exists in the cubic HoAl_3 at low temperatures, but rather other magnetic state emerges. Such successive change in magnetic state leads to the complicated behavior of ΔS_M at below T_f : ΔS_M takes small positive values for $\Delta H = 10$ kOe and 30 kOe, while it shifts to negative with further increasing ΔH .

Here let us evaluate another important magnetocaloric parameter, *i.e.*, the adiabatic temperature change ΔT_{ad} , which can also be calculated from the S - T curves as follows:

$$\Delta T_{\text{ad}}(\Delta H, T) = T(H, S) - T(0, S). \quad (2)$$

Figure 7(c) shows the ΔT_{ad} of each sample as a function of temperature for $\Delta H = 50$ kOe. For both samples, the positive ΔT_{ad} , representing the conventional MCE, is observed in the paramagnetic region, peaking a little above the T_N of each sample. The maximum value of positive ΔT_{ad} is about 2.1 K for the trigonal HoAl_3 and 3.3 K for the cubic HoAl_3 , respectively. Below T_N^{cub} , a negative ΔT_{ad} appears in the cubic HoAl_3 , indicating a decrease in temperature by adiabatic magnetization. As a consequence of the small positive ΔS_M , however, the maximum value is only about -0.4 K. For the trigonal HoAl_3 , no negative ΔT_{ad} is found below T_N^{tri} , but a small positive component is observed around 11 K, corresponding to

the hump of ΔS_M . Note that the contribution of the secondary phase (Al phase) to the specific heat, in addition to the weight fraction, may lead a decrease in the value of ΔT_{ad} observed for the samples compared to the real value for the primary phase (HoAl₃ phase), as has been pointed out in the previous work [34].

It has been proposed that potential applications of inverse MCE materials would be the cooling by adiabatic magnetization or the use as a sink for the heat generated by a conventional MCE material magnetized prior to cooling by adiabatic demagnetization [35, 36]. Nevertheless, compared to conventional MCEs, there are only a few reports on large inverse MCEs in AFM materials, especially in the low-temperature region [37–39]. Not only that, but rather a conventional MCE is often observed for a large ΔH as a result of a field-induced metamagnetic transition from an AFM state to a (forced) ferromagnetic state [37–41]. Owing to the robustness of the AFM ordering to the magnetic field, the positive ΔS_M is observed in the trigonal HoAl₃ even for $\Delta H = 50$ kOe. At the same time, however, the inverse MCE is unfortunately not so large due to its robustness. As for the cubic HoAl₃, the situation is somewhat complicated, but at least it seems unlikely that this compound is a ferromagnet with a large conventional MCE.

4. Conclusions

The magnetic, thermal, and magnetocaloric properties have been investigated for two types of HoAl₃ with different crystallographic phases. It has been found that the crystal structure of HoAl₃ is transformed by the rapid-solidification process, from the room-temperature equilibrium trigonal phase to the high-pressure cubic phase. The trigonal phase HoAl₃ is antiferromagnetically ordered at below $T_N^{\text{tri}} = 9.8$ K. The AFM ordering is so robust against the magnetic field that the inverse MCE is observed even under a large magnetic field change of 0–50 kOe. The cubic phase HoAl₃ undergoes the AFM transition at $T_N^{\text{cub}} = 15$ K, whereas the magnetic state immediately changes to a magnetic glassy state below the spin freezing temperature $T_f = 11$ K. As a consequence, the MCE exhibits complicated temperature and magnetic field dependence. Our findings demonstrate that HoAl₃ compound cannot be a promising magnetocaloric material, unlike other binary holmium aluminides.

Acknowledgements

This work was supported by JST-Mirai Program Grant Number JPMJMI18A3, Japan.

References

- [1] V. K. Pecharsky, K. A. Gschneidner, Jr., *Phys. Rev. Lett.* 78 (1997) 4494-4497.
- [2] K. A. Gschneidner, Jr., V. K. Pecharsky, A. O. Tsokol, *Rep. Prog. Phys.* 68 (2005) 1479-1539.
- [3] A. Kitanovski, J. Tusek, U. Tomc, U. Plaznik, M. Ozbolt, A. Poredos, Springer International Publishing 2015.
- [4] J. Lyubina, *J. Phys. D: Appl. Phys.* 50 (2017) 053002.
- [5] D. X. Li, T. Yamaura, S. Nimori, Y. Homma, F. Honda, Y. Haga, D. Aoki, *Solid State Commun.* 193 (2014) 6-10.
- [6] K. T. Matsumoto, K. Hiraoka, *J. Magn. Magn. Mater* 423 (2017) 318-320.
- [7] H. Zhang, R. Gimaev, B. Kovalev, K. Kamilov, V. Zverev, A. Tishin, *Physica B: Condens. Matter* 558 (2019) 65-73.
- [8] Y. Zhang, *J. Alloys Compd.* 787 (2019) 1173-1186.
- [9] P. B. Castro, K. Terashima, T. D. Yamamoto, Z. Hou, S. Iwasaki, R. Matsumoto, S. Adachi, Y. Saito, P. Song, H. Takeya, Y. Takano, *NPG Asia Mater.* 12 (2020) 35.
- [10] L. Li, M. Yan, *J. Alloys Compd.* 823 (2020) 153810.
- [11] H. Omote, S. Watanabe, K. Matsumoto, I. Gilmutdinov, A. Kiiamov, D. Tayuskii, *Cryogenics* 101 (2019) 58-62.
- [12] L. Li, P. Xu, S. Ye, Y. Li, G. Liu, D. Hou, M. Yan, *Acta Mater.* 194 (2020) 354-365.
- [13] B. Wu, Y. Zhang, D. Guo, J. Wang, Z. Ren, *Cer. Int.* 47 (2021) 6290-6297.
- [14] P. Xu, Z. Ma, P. Wang, H. Wang, L. Li, *Mat. Today Phys.* 20 (2021) 100470.
- [15] Y. Zhang, Y. Tian, Z. Zhang, Y. Jia, B. Zhang, M. Jiang, J. Wang, Z. Ren, *Acta Mater.* 226 (2022) 117669.
- [16] T. Hashimoto, K. Matsumoto, T. Kurihara, T. Numazawa, A. Tomokiyo, H. Hayama, T. Goto, S. Todo, M. Shahari, *Adv. Cryog. Eng. Mater.* 32 (1986) 279-286.

- [17] L. H. Yang, H. Zhang, F. X. Hu, J. R. Sun, L. Q. Pan, B. G. Shen, *J. Alloys Compd.* 596 (2014) 58-62.
- [18] H. Zhang, Z. Y. Xu, X. Q. Zheng, J. Shen, F. X. Hua, J. R. Sun, B. G. Shen, *Solid State Commun.* 152 (2012) 1127-1130.
- [19] A. Bhattacharyya, S. Giri, S. Majumdar, *J. Phys.: Condens. Matter* 22 (2010) 316003.
- [20] J. H. N. Van Vucht, K. H. J. Buschow, *J. Less-Common Metals* 10 (1965) 98-107.
- [21] J. F. Cannon, H. T. Hall, *J. Less-Common Metals* 40 (1975) 313-328.
- [22] K. H. J. Buschow, Rare earth compounds, in: E. P. Wohlfarth (Ed.), *Handbook of Ferromagnetic Materials*, vol. 1, Elsevier, 1980, pp. 297-414.
- [23] M. Sahashi, H. Niu, Y. Tohkai, K. Inomata, T. Hashimoto, T. Kuzuhara, A. Tomokiyo, H. Yamaya, *IEEE Trans. Magn.* 23 (1987) 2853-2855.
- [24] K. Momma, F. Izumi, *J. Appl. Crystallogr.* 44 (2011) 1272.
- [25] Y. Xu, Z. Altounian, W. B. Muir, *Appl. Phys. Lett.* 58 (1991) 125-127.
- [26] A. Meyer, *J. Less-Common Metals* 10 (1966) 121-129.
- [27] P. B. Castro, K. Terashima, M. G. E. Echevarria, H. Takeya, Y. Takano, *Adv. Theory and Simul* (2021): 2100588.
- [28] W. J. Hu, J. Du, B. Li, Q. Zhang, Z. D. Zhang, *Appl. Phys. Lett.* 92 (2008) 192505.
- [29] M. Khan, D. Paudyal, K. A. Gschneidner, Jr., V. K. Pecharsky, *J. Appl. Phys.* 113 (2013) 17E106.
- [30] J. A. Mydosh, *Rep. Prog. Phys.* 78 (2015) 052501.
- [31] J. H. Schelleng, S. A. Friedberg, *J. Appl. Phys.* 34 (1963) 1087-1089.
- [32] A. Biswas, S. Chandra, T. Samanta, M. H. Phan, I. das, H. Srikanth, *J. Appl. Phys.* 113 (2013) 17A902.
- [33] P. J. Von Ranke, N. A. de Oliveira, B. P. Alho, E. J. R. Plaza, V. S. R. de Sousa, L. Caron, M. S. Reis, *J. Phys.: Condens. Matter* 21 (2009) 056004.
- [34] T. D. Yamamoto, H. Takeya, K. Terashima, S. Iwasaki, P. B. Castro, T. Numazawa, Y. Takano, *J. Magn. Mater.* 513 (2020) 167207.

- [35] R. J. Joenk, *J. Appl. Phys.* 34 (1963) 1097-1098.
- [36] T. Krenke, E. Duman, M. Acet, E. F. Wassermann, X. Moya, L. Mañosa, A. Planes, *Nat. Mat.* 4 (2005) 450-454.
- [37] R. D. does Reis, L. M. da Silva, A. O. dos Santos, A. M. N. Medina, L. P. Cardoso, F. G. Gandra, *J. Phys.: Condens. Matter* 22 (2010) 486002.
- [38] W. Zuo, F. Hu, J. Sun, B. Shen, *J. Alloys Compd.* 575 (2013) 162-167.
- [39] X. Q. Zheng, Z. Y. Xu, B. Zhang, F. X. Hu, B. G. Shen, *J. Magn. Magn. Mater.* 421 (2017) 448-452.
- [40] J. Chen, B. G. Shen, Q. Y. Dong, J. R. Sun, *Solid State Commun.* 150 (2010) 1429-1431.
- [41] Y. Zhang, Y. Yang, C. Hou, D. Guo, X. Li, Z. Ren, G. Wilde, *Intermetallics* 94 (2018) 17-21.

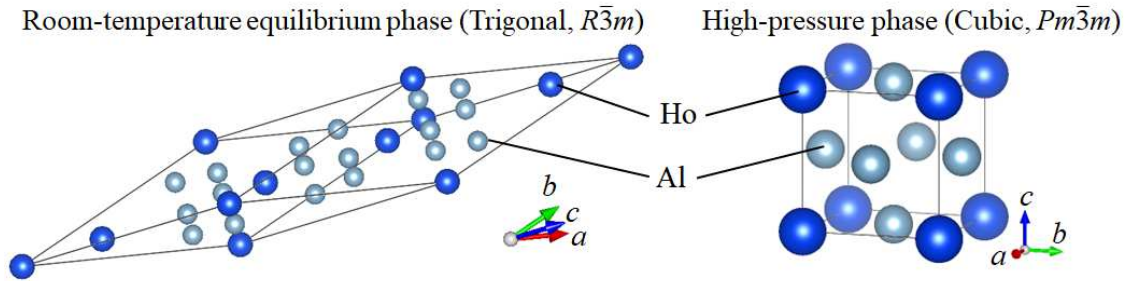


Figure 1: (Color Online) Crystal structures of HoAl_3 , drawn using VESTA [24].

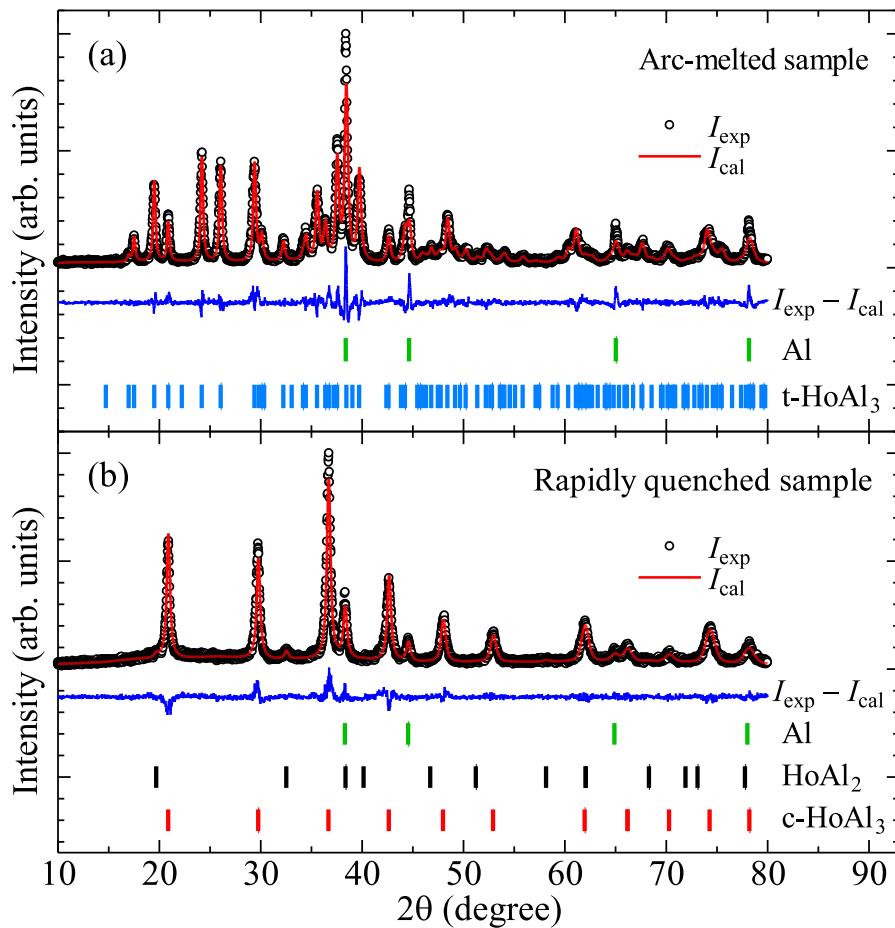


Figure 2: (Color Online) Powder XRD patterns of the arc-melted HoAl_3 (a) and the rapidly quenched HoAl_3 (b) along with Rietveld refinement. The bars represent the Bragg peak positions of individual phases. The t- HoAl_3 and the c- HoAl_3 indicate trigonal phase HoAl_3 and cubic phase HoAl_3 , respectively.

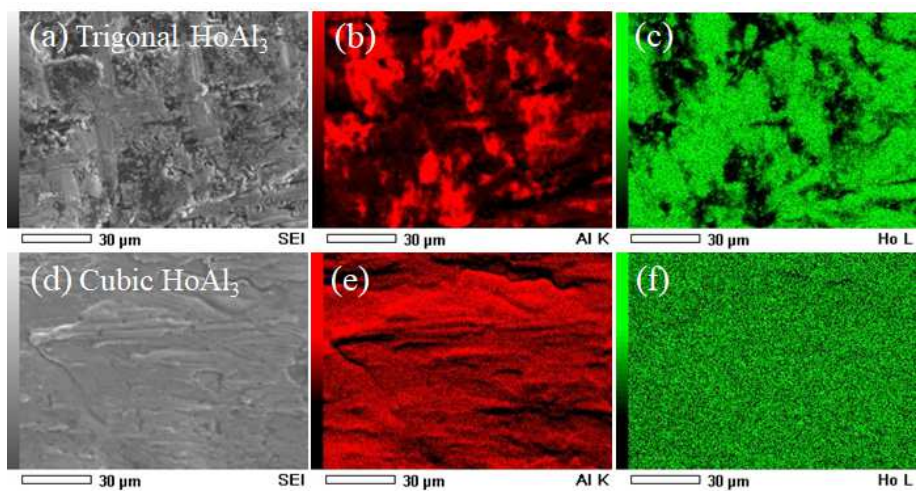


Figure 3: (Color Online) (a)-(c) SEM secondary electron image (a) of the trigonal HoAl_3 and the corresponding EDS mapping images for Al (b) and Ho (c) elements. (d)-(f) Those of the cubic HoAl_3 .

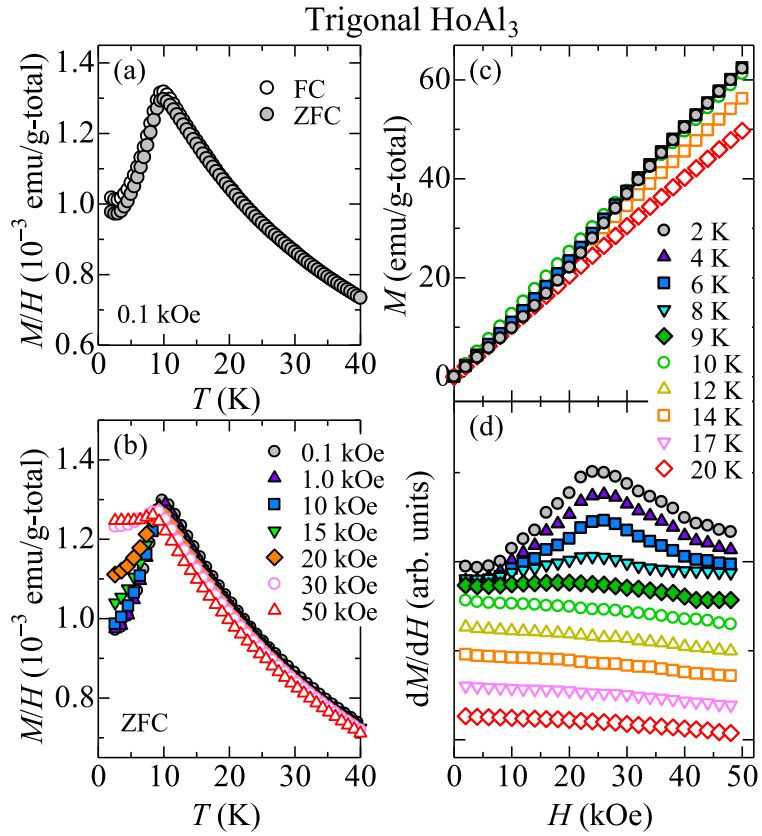


Figure 4: (Color Online) Magnetic Properties of the trigonal HoAl₃. (a) The temperature dependence of the magnetic susceptibility (M/H - T curve) at 0.1 kOe in ZFC and FC processes. (b) M/H - T curves under various magnetic fields in ZFC processes. (c)-(d) Field dependence of the magnetization M (c) and the field derivative dM/dH (d) at various temperatures.

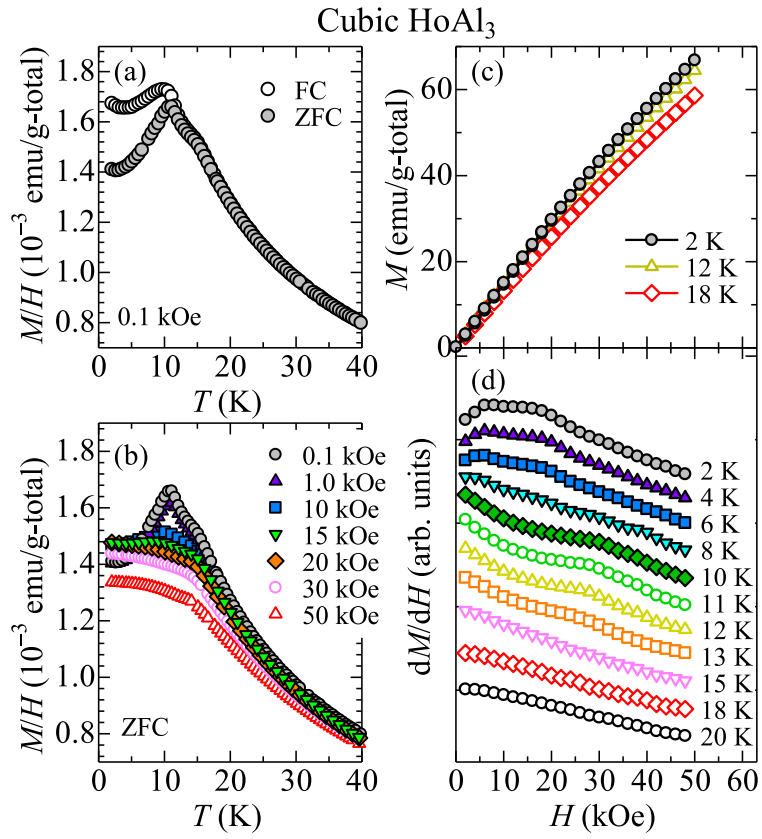


Figure 5: (Color Online) Magnetic Properties of the cubic HoAl₃. (a) M/H - T curves at 0.1 kOe in ZFC and FC processes. (b) M/H - T curves under various magnetic field in ZFC processes. (c)-(d) Field dependence of M (c) and dM/dH (d) at various temperatures.

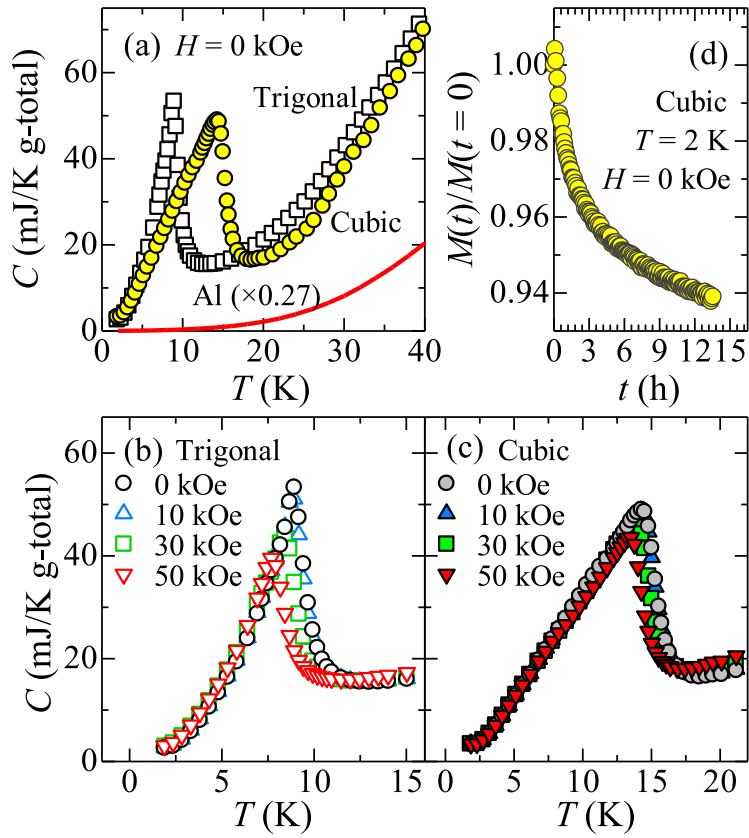


Figure 6: (Color Online) (a) Temperature dependence of the specific heat C at 0 kOe for the trigonal HoAl₃ and the cubic HoAl₃. The solid line represents C of aluminum scaled by the weight fraction of 0.27. (b)-(c) C under several magnetic fields in the trigonal HoAl₃ (b) and the cubic HoAl₃ (c). (d) Magnetic relaxation curve at 2 K at 0 kOe in the cubic HoAl₃.

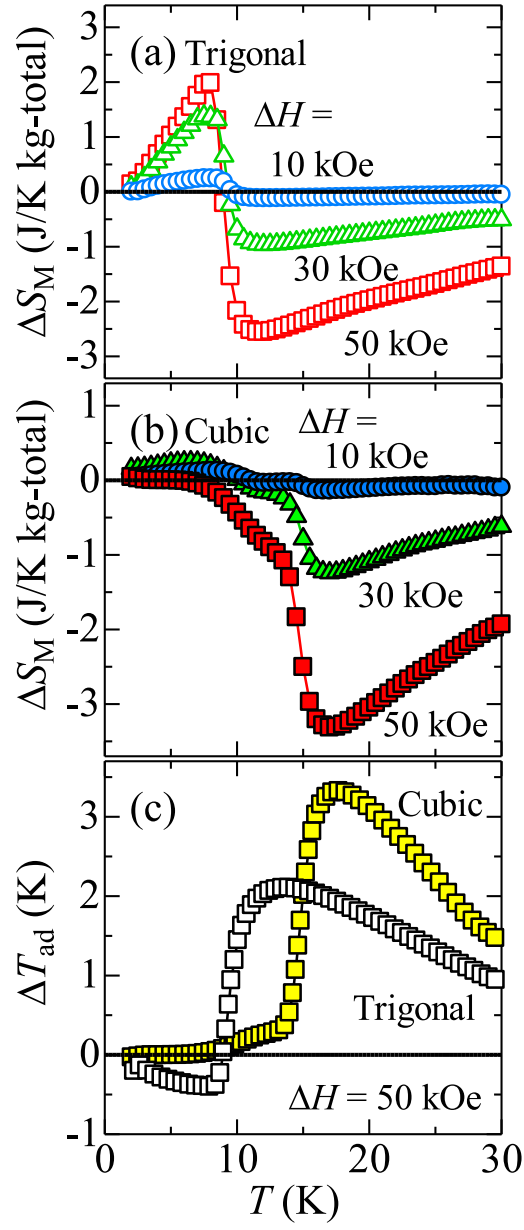


Figure 7: (Color Online) (a)-(b) Magnetic entropy change ΔS_M of the trigonal HoAl_3 (a) and the cubic HoAl_3 (b) for the magnetic field change $\Delta H = 10, 30,$ and 50 kOe. (c) Adiabatic temperature change ΔT_{ad} of the samples for $\Delta H = 50$ kOe.